Process Damping Coefficient Identification using Bayesian Inference

Jaydeep M. Karandikar, Christopher T. Tyler, and Tony L. Schmitz
Mechanical Engineering and Engineering Science
University of North Carolina at Charlotte
Charlotte, NC

ABSTRACT
This paper describes the application of the random walk method for Bayesian inference to the identification of the process damping coefficient in milling. An analytical process damping algorithm is used to model the prior distribution of the stability boundary and it is updated using experimental results via Bayesian inference. The updated distribution of the stability boundary is used to determine the posterior process damping coefficient value. The method is validated by comparing the process damping posterior values to residual sum of squares results. A value of information approach for experimental test point selection is demonstrated which minimizes the number of experiments required for process damping coefficient identification.

KEYWORDS
Milling, process damping, Bayesian inference, value of information

INTRODUCTION

The analytical stability lobe diagram offers an effective predictive capability for selecting stable chip width-spindle speed combinations in machining operations [1-4]. However, the increase in allowable chip width provided at spindle speeds near integer fractions of the system's dominant natural frequency is diminished substantially at low spindle speeds where the stability lobes are closely spaced. However, the process damping effect can serve to increase the chatter-free chip widths at these low speeds. This increased stability at low spindle speeds is particularly important for hard-to-machine materials that cannot take advantage of the higher speed stability zones due to prohibitive tool wear at high cutting speeds.

Many researchers have investigated process damping in turning and milling operations. Seminal studies were carried out by Wallace and Andrew [5], Sisson and Kegg [6], Peters *et al.* [7], and Tlusty [8]. It was demonstrated by this early work that interference contact between the flank of the cutting tool and wavy cutting surface contributes to the process damping phenomenon.

The increased use of exotic, hard-to-machine alloys has driven recent efforts to accurately predict process damping behavior. Wu [9] developed a model in which plowing forces present during the tool-workpiece contact are assumed to be proportional to the volume of interference between the cutter flank face and undulations on the workpiece surface in turning.

Elbestawi and Ismail [10], Lee *et al.* [11], Huang and Wang [12], and Ahmadi and Ismail [13] extended Wu's force model to milling operations. Budak and Tunc [14] and Altintas *et al.* [15] experimentally identified different dynamic cutting force models to include process nonlinearities and incorporate process damping. Tyler and Schmitz [16] described an analytical approach to establish the stability boundary that includes process damping effects in turning and milling operations using a single process damping coefficient.

These studies described process damping as energy dissipation due to interference between the cutting tool clearance face and machined surface during relative vibrations between the tool and workpiece. It was shown that, given fixed system dynamics, the influence of process damping increases at low spindle speeds because the number of undulations on the machined surface between revolutions/teeth increases, which also increases the local slope of the wavy surface. This, in turn, leads to increased interference and additional energy dissipation.

This paper extends the work performed by Tyler and Schmitz [16] and demonstrates a Bayesian updating method to efficiently identify the process damping model parameters. In the first section, process damping is described and the results presented in [16] are summarized. Next, the Bayesian updating method used to determine the process damping coefficient is described

and validated by comparing the results to those obtained using the residual sum of squares (RSS) method described in [16]. A value of information approach is then presented for experimental test point selection; this is followed by conclusions.

PROCESS DAMPING DESCRIPTION

To describe the physical mechanism for process damping, consider a tool moving on a sine wave while shearing away the chip [16]; see Fig. 1. Four locations are identified: 1) the clearance angle, γ, between the flank face of the tool and the work surface tangent is equal to the nominal relief angle for the tool; 2) γ is significantly decreased and can become negative (which leads to interference between the tool's relief face and surface); 3) γ is again equal to the nominal relief angle; and 4) γ is significantly larger than the nominal value.

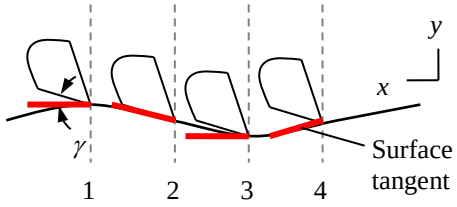

Figure 1. Physical description of process damping. The clearance angle varies with the instantaneous surface tangent as the tool removes material on the sinusoidal surface.

At points 1 and 3 in Figure 1, the clearance angle is equal to the nominal value so there is no effect due to cutting on the sinusoidal path. However, at point 2 the clearance angle is small (or negative) and the thrust force in the surface normal direction is increased. At point 4, on the other hand, the clearance angle is larger than the nominal and the thrust force is decreased. Because the change in force caused by the sinusoidal path is 90 deg out of phase with the displacement and has the opposite sign from velocity, it is considered to be a viscous damping force (i.e., a force that is proportional to velocity).Given the preceding description, the process damping force, F_d, in the y direction can be expressed as a function of velocity, $\dot{y}$, chip width, b, cutting speed, V, and a process damping constant C [15]. See Eq. 1.

$$F_d = -C\frac{b}{V}\dot{y} \tag{1}$$

Because the new damping value is a function of both the spindle speed-dependent limiting chip width and the cutting speed, the b and Ω vectors must be known in order to implement the new damping value. This leads to a stability analysis that incorporates process damping. The following steps are completed for each lobe in the stability lobe diagram:

1. the analytical stability boundary is calculated with no process damping ($C = 0$) to identify initial b and Ω vectors
2. these vectors are used to determine the corresponding new damping coefficient vector (which includes both the structural damping and process damping, $C \neq 0$)
3. the stability analysis is repeated with the new damping coefficient vector to determine the updated b and Ω vectors
4. the process is repeated until the stability boundary converges.

The automated algorithm description and validation are described in [16]. Figure 2 illustrates a comparison between stability lobes diagram developed with and without process damping for a selected C value.

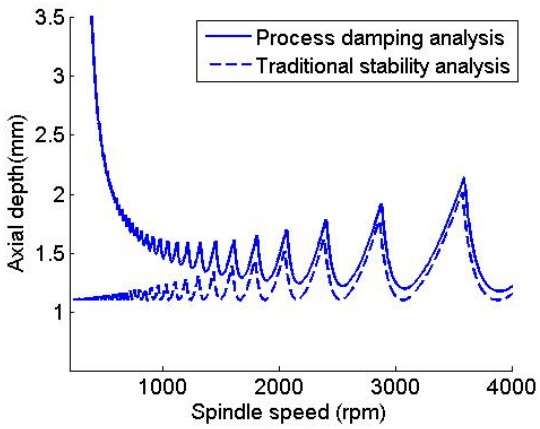

Figure 2. Comparison between process damping stability lobes and traditional stability lobes.

EXPERIMENTAL IDENTIFICATION OF PROCESS DAMPING COEFFICIENT

In order to provide convenient control of the system dynamics, a single degree-of-freedom, parallelogram leaf-type flexure was constructed to provide a flexible foundation for individual AISI 1018 steel workpieces; see Figure 3. Because the flexure compliance was much higher than the tool-holder-spindle-machine, the stability analysis was completed using only the flexure's dynamic properties. A radial immersion of 50% and a feed per tooth of 0.05 mm/tooth was used for all conventional (up) milling tests.

An accelerometer (PCB Piezotronics model 352B10) was used to measure the flexure's vibration during cutting. The frequency content of the accelerometer signal was used in combination with the machined surface finish to establish stable/unstable performance, i.e., cuts that exhibited significant frequency content at the flexure's compliant direction natural frequency, rather than the tooth passing frequency and its harmonics, were considered to be unstable.

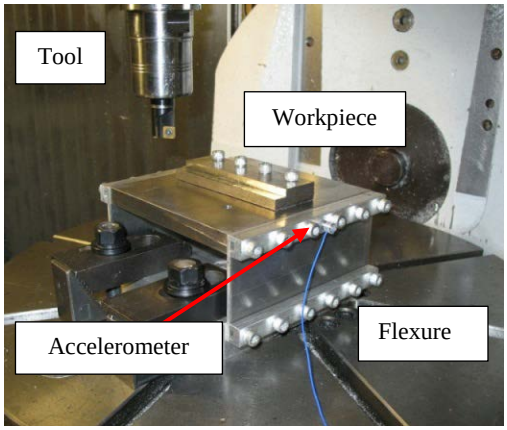

Figure 3. Setup for milling stability tests. An accelerometer was used to measure the vibration signal during cutting.

Process Damping Coefficient Identification

A grid of test points at low spindle speeds was selected to investigate the process damping behavior. Based on the stable/unstable cutting test results, a single variable residual sum of squares (RSS) estimation was applied to identify the process damping coefficient that best represented the experimental limiting axial depth of cut, b_{lim}. This method is described in detail in [16].

The results of the coefficient identification method are depicted in Figure4 for an18.54mm diameter, single-tooth inserted endmill with a 15deg relief angle. For the same milling conditions and system dynamics, the process was repeated for a 19.05 mm diameter, single-tooth inserted endmill with an 11deg relief angle. The stability boundary for this experiment is provided in Figure5. The corresponding process damping coefficients and cutting force coefficients in the tangential, *t*, and normal, *n*, directions (as defined in [18]) are provided in Table 1. For these tests, the insert wear was monitored using in-process optical flank wear measurements and the insert was replaced if the wear exceeded a predetermined value.

From Figures 4and 5 it can be observed that numerous cutting tests were used to identify the process damping coefficient for a particular cutting operation. This can be costly if there are multiple cutter geometries/workpiece materials for which stability boundaries need to be constructed. The following section details a Bayesian updating method for optimizing the experimental test selection and determining the process damping coefficient more efficiently.

Table 1. Comparison of process damping and cutting force coefficients for different relief angle cutters.

Relief angle (deg)	C (N/m)	K_t (N/mm^2)	K_n (N/mm^2)
15	2.5×10^5	2111.2	1052.6
11	3.3×10^5	2234.9	1188.2

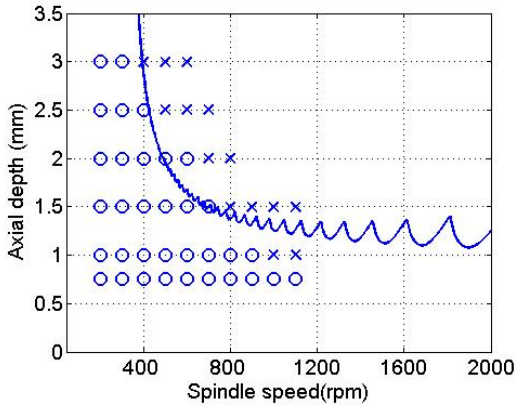

Figure 4. Up milling stability boundary for 50% radial immersion, 18.54 mm diameter, 15deg relief angle, low wear milling tests using the 228 Hz flexure setup ($C = 2.5\times10^5$ N/m).

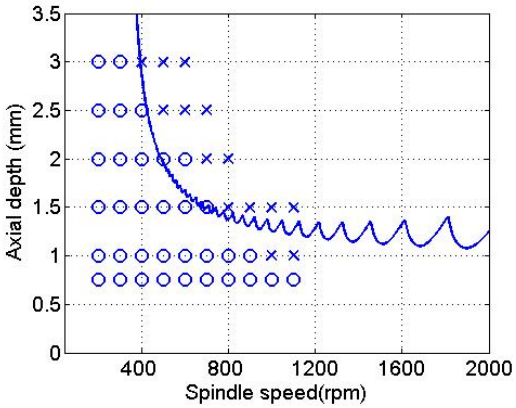

Figure 5. Up milling stability boundary for 50% radial immersion, 19.05 mm diameter, 11deg relief angle, low wear milling tests using the 228 Hz flexure setup ($C = 3.3\times10^5$ N/m).

BAYESIAN UPDATING OF THE PROCESS DAMPING COEFFICIENT

This section describes the Bayesian updating method for process damping coefficient identification. The updating was performed using the experimental results shown in Figures 4 and 5. In these figures, uncertainty exists in the true location of the stability boundary due to the uncertainties/assumptions in the process damping model and its parameters as well as factors that are not known. Therefore, the stability boundary may be modeled as a cumulative probability distribution rather than a deterministic boundary. From a Bayesian standpoint, an uncertain variable is treated as random and is characterized by a probability distribution. Bayesian inference is a normative and formal method of belief updating when new information (e.g., experimental stability results) is made available.

The stability boundary prediction proceeds by generating n sample paths, each of which may represent the actual stability boundary with some probability. For the prior (or initial belief), each path is assumed to be equally likely to be the true stability limit. Therefore, the probability that each sample path is the true stability limit is $1/n$. These sample paths are used as the prior in applying Bayesian inference.

Bayesian updating was used to update the prior probability of sample paths given experimental result, and therefore, the process damping coefficient distribution. The entire methodology is defined as Bayesian updating using a random walk approach. Bayes' rule is given by Eq. 2.

$$P(path = true\ stability\ limit \mid test\ result) \propto P(test\ result \mid path = true\ stability\ limit)\, P(path = true\ stability\ limit) \quad (2)$$

Here, $P(path = true\ stability\ limit)$ is the prior probability that a selected path is the true stability limit; before any testing; it is equal to $1/n$ for any sample path. Also, $P(test\ result \mid path = true\ stability\ limit)$ is the likelihood of obtaining the test result given the true stability limit. Their products yields the posterior probability that a selected path is the true path given the test result, $P(path = true\ stability\ limit \mid test\ result)$. In practice, the probability of the test result, $P(test\ result)$, may be used to normalize the posterior probability (by dividing the right hand side of Eq. 2 by this value). The sample paths are generated by randomly sampling from the prior distributions of the K_t, K_n, and C values and calculating a stability boundary for each set.

Establishing the prior

The random sample stability limits are generated by sampling from the prior distributions of K_t, K_n, and C. To demonstrate the approach, the 18.54 mm diameter, 11 deg relief angle tool is considered. The distribution of C is not known and has to be determined. The prior marginal distribution of C was selected to be the uniform distribution $U(0.5\times10^5,\ 10\times10^5)$, where the values in the parenthesis specify the lower and upper limits on C, respectively. A uniform distribution denotes that it is equally likely for the value of C to be between 0.5×10^5 N/m and 10×10^5 N/m and represents a non-informative case where little prior knowledge of the variable is available. Recall that the value of C for the 18.54 mm diameter, 15 deg relief angle tool was found to be 2.5×10^5 N/m using the RSS method (see Figure 4). The values of K_t and K_n were calculated using a linear least squares fit to the mean forces in the x (feed) and y directions at different feed per tooth values. The mean and standard deviation of the force coefficients were calculated from three measurement sets. Based on this data, the marginal prior distributions of the force coefficients were $K_t = N(2111.2, 78.3)$ N/mm^2 and $K_n = N(1052.6, 27.9)$ N/mm^2, where N denotes a normal distribution and the terms in parenthesis specify the mean and standard deviation, respectively. The prior distributions of K_t, K_n, and C were assumed to be independent of each other. Random samples are drawn from the prior distributions and the stability limit was calculated for each sample. Figure 6 shows the prior cumulative distribution function (cdf) for probability of stability. The maximum possible axial depth of cut possible was defined as 7.5 mm based on the tool's cutting edge length. Figures7 and 8 show the probability of stability, p(stability), as a function of axial depth at 400 rpm and 1000 rpm, respectively. As expected, the probability of stability decreases at higher axial depths at a given spindle speed. For example, the probability of stability at 1 mm is 1 at both speeds, while the probability of stability for an axial depth of 4 mm is 0.7 at 400 rpm and only 0.25 at 1000 rpm.

Likelihood function

The likelihood function describes how likely the test result is given that the sample path is the true stability limit. The likelihood function incorporates the uncertainty in the process damping model and, therefore, the stability boundary. To illustrate, consider an experiment completed at a spindle speed of 1000 rpm and an axial depth of 3 mm. A stable result indicates that the test result is equally likely for all paths that have an axial depth greater than 3 mm at 1000 rpm; they are assigned a likelihood of unity. On the other hand, a stable result at 3 mm is unlikely for all paths with an axial depth less than 3 mm at 1000 rpm. Note that the stable result is unlikely but not impossible for such paths, giving a nonzero likelihood. As shown in Figures 4 and 5, stable points may lie above the boundary and unstable points may lie below the boundary since there is uncertainty in the stability boundary location.

Note that the test result is increasingly unlikely for values less than 3 mm at 1000 rpm. For example, the test result is more unlikely for a path that has a value of 1 mm at 1000 rpm relative to a path that has a value of 2.5 mm at 1000 rpm. Therefore, the likelihood is a one-sided function. The likelihood function for a stable result is described by Eq. 3.

$$l = e^{\frac{-(b-b_{test})^2}{k}} \quad b < b_{test} \qquad l = 1 \quad b \geq b_{test} \tag{3}$$

The likelihood function is expressed as a non-normalized normal distribution, where the parameter $k = 2\sigma^2$ and σ is the standard deviation in the axial depth due to the model uncertainty. The value of σ was taken to be 0.5 mm. Similarly, an unstable cut indicates that test result is likely for all paths that have an axial depth value less than 3 mm at 1000 rpm, while it is unlikely for all paths that have a value greater than 3 mm. Although a Gaussian kernel is used in this study, it can be any function defined by the user based on his/her beliefs.

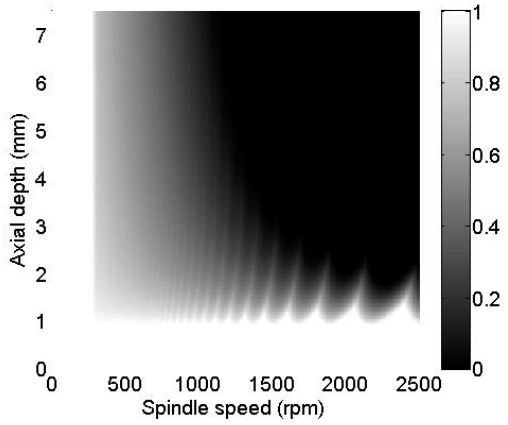

Figure 6. Prior cdf of stability. The gray color scale represents the probability of stability for any spindle speed, axial depth combination (1/white is likely to be stable, while 0/black is unlikely to be stable).

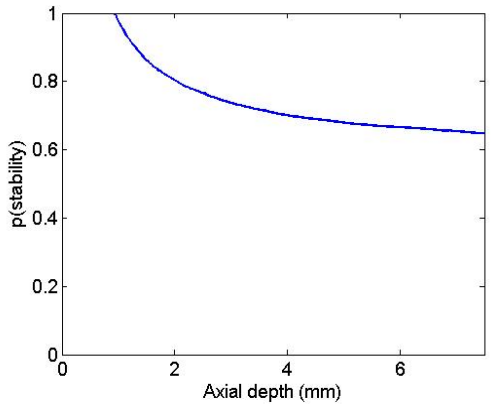

Figure 7. Probability of stability at 400 rpm.

The likelihood function for an unstable result is provided in Eq. 4. Figure 9 displays the likelihood function for a stable result at 3 mm and Figure 10 shows the likelihood for an unstable result.

$$l = 1 \quad b < b_{test} \qquad l = e^{\frac{-(b-b_{test})^2}{k}} \quad b \geq b_{test} \tag{4}$$

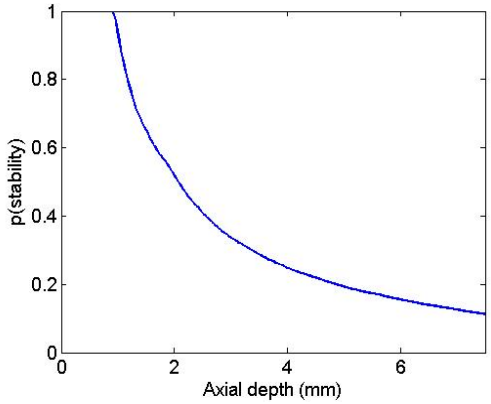

Figure 8. Probability of stability at 1000 rpm.

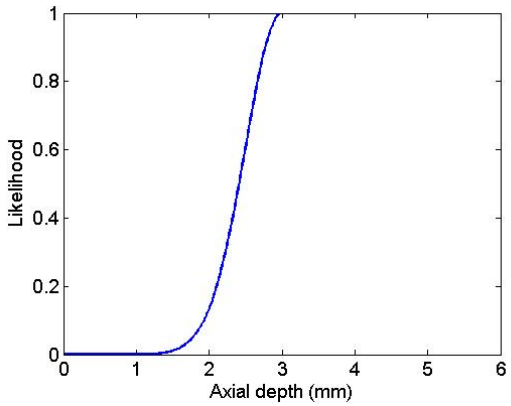

Figure 9. Likelihood given a stable result at 3 mm.

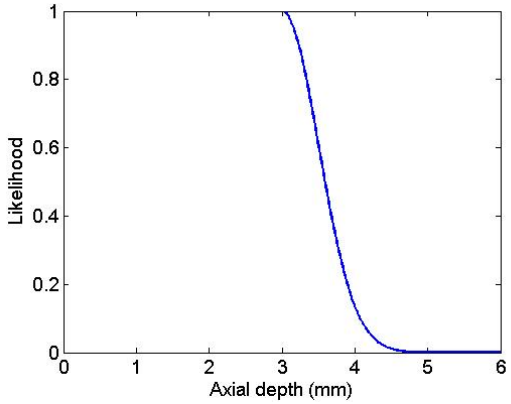

Figure 10. Likelihood given an unstable result at 3 mm.

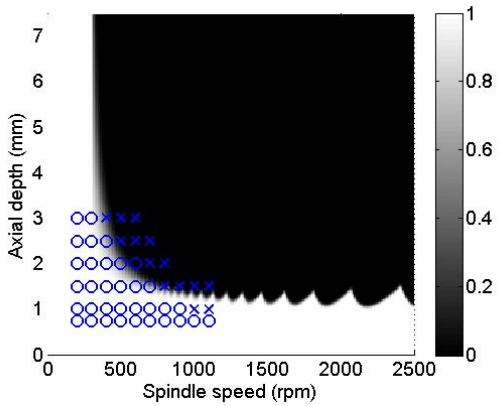

Figure 11. Posterior cdf of stability. Stable results are denoted as 'o' and unstable results as 'x'.

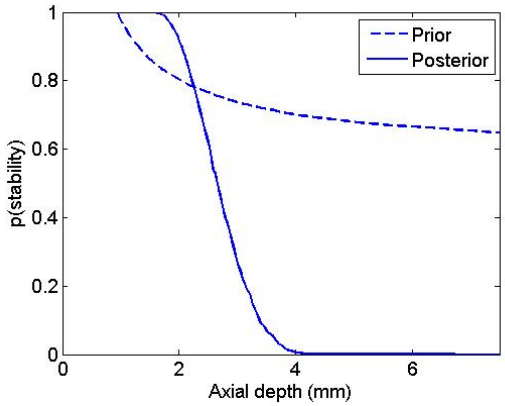

Figure 12. Prior and posterior probability of stability at 400 rpm.

Bayesian updating

The posterior probability of each path is obtained by multiplying the prior and likelihood and normalizing such that the sum of all probabilities is equal to unity. The posterior probabilities of sample paths are used to calculate the posterior distribution of the process damping and cutting force coefficients. The experimental results shown in Figure 4 were used to update the prior cdf of stability. For each experiment, the likelihood function was calculated using Eqs. 3 and 4 for a stable and unstable result, respectively. For multiple updates, the prior after the first update becomes the posterior after the second update and so on. Figure 11 shows the posterior cdf given the experimental results. Stable results are denoted as 'o' and unstable results as 'x'. Figure 12 and Figure 13 shows the prior and posterior probability of stability at 400 rpm and 1000 rpm, respectively.

After each update, the posterior mean and standard deviation of C was calculated using Eqs. 5 and 6.

$$\mu_C = \sum C\mathrm{P}(C) \tag{5}$$

$$\sigma_C = \sum (C - \mu_C)^2 \mathrm{P}(C) \tag{6}$$

In these equations, μ_C and σ_C are the mean and standard deviation of C, respectively, and P(C) is the probability of the sample stability limit. Recall that each sample stability limit is generated from a sample of {K_t, K_n, C}. The probability of a sample stability limit is equal to the probability that the sample is the true limit.

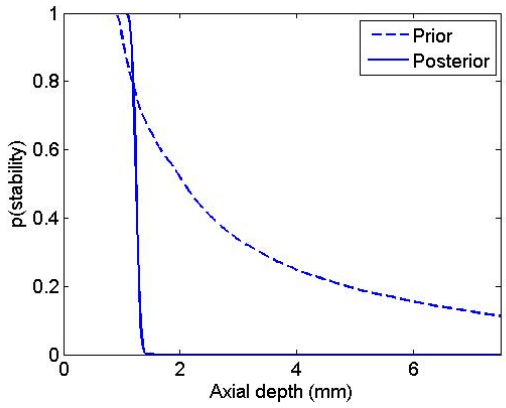

Figure 13. Prior and posterior probability of stability at 1000 rpm.

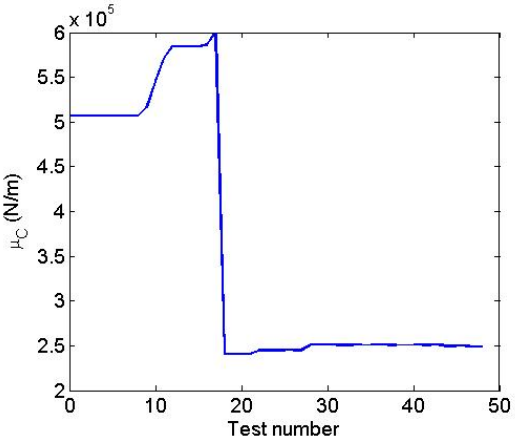

Figure 14. μ_C as a function of the number of tests.

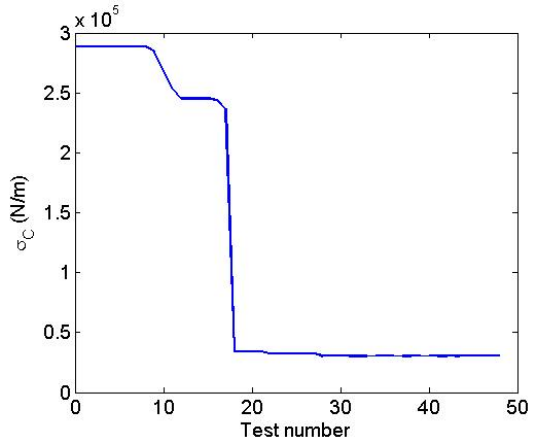

Figure 15. σ_C as a function of the number of tests.

For the prior, each sample stability limit was assumed to be equally likely to be the true limit; this implies that each $\{K_t, K_n, C\}$ sample was equally likely to be the true combination. The updated probability of each sample stability limit gives the updated probability of the underlying $\{K_t, K_n, C\}$ sample to be the true combination. The updated posterior probabilities of sample paths were used to calculate the posterior mean and standard deviation of C using Eqs. 5 and 6, respectively. Figures 14 and 15 show the progression of μ_C and σ_C as a function of the number of tests.

The μ_C and $\sigma_C$values after 48 tests were 2.49×10^5 N/m and 0.30×10^5 N/m, respectively. The value of C from the RSS method was 2.5×10^5 N/m. Figures14and 15show a convergence in μ_C and σ_C to the final values after the 18th test. The μ_C and $\sigma_C$values after the 18th test were 2.41×10^5 N/m and 0.34×10^5 N/m, respectively. This is due to the first unstable result at {400 rpm, 3 mm axial depth} preceded by a stable result at {400 rpm, 2.5 mm axial depth}. A stable result at a 2.5 mm axial depth and an unstable result at a 3 mm axial depth imply that there is a high probability that the true stability limit is between the two values. Also, note that the values remain approximately constant after subsequent updates.

The updating procedure was repeated for the 19.05 mm diameter, 11 deg relief angle tool. The prior marginal distribution of the force coefficients were $K_t = N(2234.9, 107.0)$ N/mm^{2}and $K_n = N(1188.2, 40.5)$ N/mm^2.The prior marginal distribution of C was again selected to be uniform, $U(0.5\times10^5, 10\times10^5)$ N/m, and the coefficients were assumed to be independent of each other. The updating procedure was performed using the experimental results shown in Figure 5. Figure 16 shows the posterior cdf given experimental results. Figures 17 and 18 show the progression of μ_C and σ_C as a function of the number of tests. The μ_C and σ_C values after 55 tests were 3.63×10^5N/m and 0.38×10^5N/m, respectively. The C value from the RSS method was 3.3×10^5 N/m.

These results show good agreement between the posterior mean C and the value obtained using the RSS method. The advantage of using Bayesian inference over RSS is that the uncertainty in C can also be calculated. As a result, the stability boundary is not deterministic, but characterized by a cumulative probability distribution. In addition, Bayesian inference enables the value to be gained from performing an experiment to be calculated; this is described in the next section.

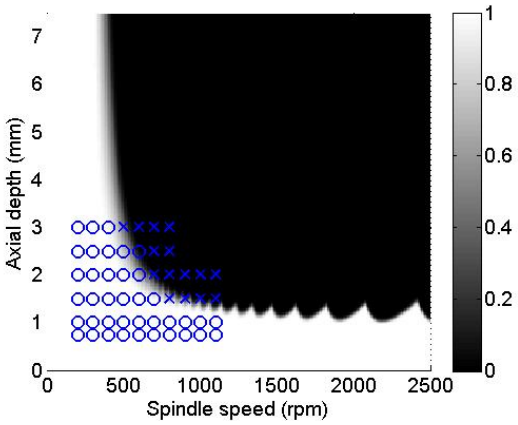

Figure 16. Posterior cdf of stability. Stable results are denoted as 'o' and unstable results as 'x'.

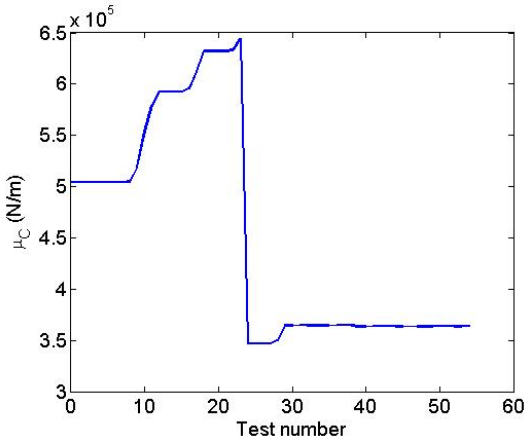

Figure 17. μ_C as a function of the number of tests.

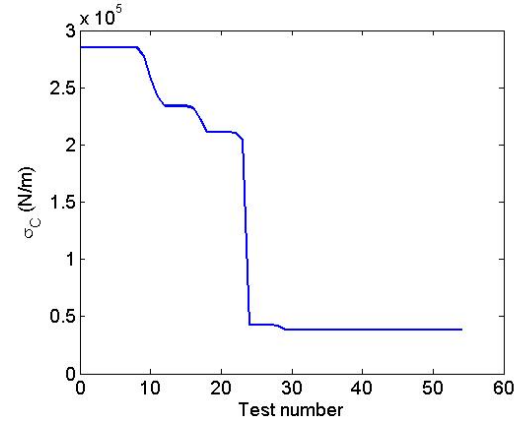

Figure 18. σ_C as a function of the number of tests.

EXPERIMENTAL PARAMETER SELECTION

Bayesian updating of the probability of stability and the process damping coefficient was demonstrated. Using experimental results, the probability of each sample stability limit being the true limit was updated. These probabilities were, in turn, used to determine the posterior distribution of the process damping coefficient. The posterior mean agreed with the deterministic value calculated using the RSS method. Note that additional experimental results reduce the uncertainty (or the standard deviation) in the *C* value.

This section describes a value of information approach for optimal experimental parameter selection. The objective of the experiments is to reduce the uncertainty in the *C* value. Note that no new information (or reduction in uncertainty) is achieved by obtaining a stable result at a {spindle speed, axial depth} combination which has a probability of stability equal to one. A probability of stability equal to one indicates that all sample paths have a value of axial depth greater than the test axial depth at the test spindle speed. A stable result assigns a likelihood of one to all the sample stability limits, which results in no reduction in the value of σ_C. This is observed in Figures 15 and 18 for the first five tests. On the other hand, a test at a combination which has a non-zero probability of stability will cause a reduction in σ_C due to the small likelihood value assigned to some sample paths.

The information from a test is characterized as an expected percent reduction in the value of σ_C. The experimental parameters are selected where the expected percent reduction in σ_C is maximum. To illustrate, consider four possible experimental {spindle speed, axial depth} combinations: A= {400 rpm, 1.28 mm}, B = {1000 rpm, 2.68 mm}, C = {1500 rpm, 2.04 mm} and D = {2000 rpm, 1.36 mm}. The probability of stability for test points A, B, C and D are 0.9, 0.5, 0.1, and 0.52, respectively (see Figure 19).

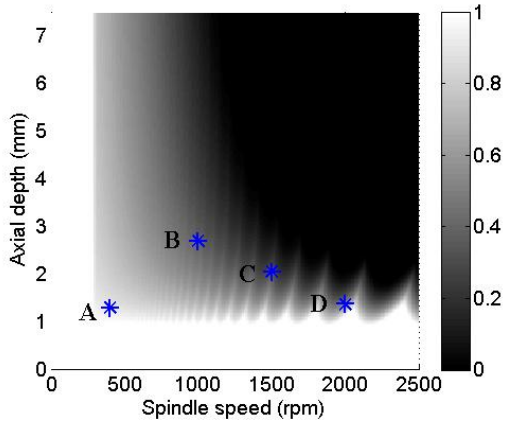

Figure 19. Four possible test points.

Consider test point A. Given a stable or unstable result at point A, the posterior probabilities of the sample stability limits is updated using the procedure described previously. The posterior probabilities are used to calculate the values of μ_C of and σ_C via Eqs. 3 and 4. If the result at point A is stable, the value of σ_C would be 2.72×10^5 N/m. Note that the value of σ_C before any testing was 2.87×10^5 N/m. Therefore, the percent reduction in σ_C would be 5.60. On the other hand, if the result at point A was unstable, the value of σ_C would be 3.47×10^4 N/m giving a percent reduction of 87.9. Recall that point A has a 0.9 probability of being stable. The expected percent reduction in σ_C for point A is calculated as:

(% reduction in $\sigma_C)_A = 0.9\times5.60 + 0.1\times87.9 = 13.8$.

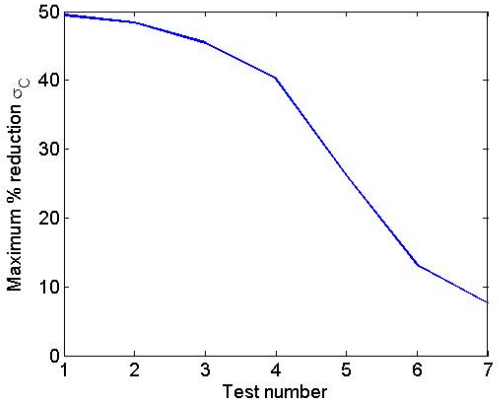

Figure 20. Maximum expected percent reduction for each test.

The procedure was repeated for points B, C and D. The results are summarized in Table 2. As noted, points A and C have a high prior probability of being stable and unstable, respectively. As a result, the expected percent reduction in σ_C for testing at these points is low. On the other hand, points B and D have maximum uncertainty regarding the result, p(stability) = 0.5. Also, the uncertainty in the probability of stability is higher at point B as compared to point D. Therefore, the expected percent reduction is greater for testing at point B than point D.

The {spindle speed, axial depth} domain was divided into a grid with increments of 50 rpm and 0.15 mm. The expected percent reduction in σ_C was calculated at all grid points using the procedure described. The maximum expected percent reduction was 49.6 at {550 rpm, 7.5 mm) with a probability of stability equal to 0.51. The test result was selected to be unstable based on the stability limit shown in Figure 4. The purpose of using the stability limit in Figure 4 to determine the test result was to validate the convergence of the posterior mean and standard deviation of *C* to the values determined using the original 48 tests. The values of μ_C and σ_C after the first update were 2.53×10^5 N/m and 1.42×10^5 N/m, respectively. The posterior after the first update becomes the prior for the second update. The procedure was repeated for seven tests (all based on the stability limit shown in Figure 4). The test points were selected where the expected percent reduction in *C* was maximum. Figure 20 shows the maximum expected percent reduction in *C* for each test. As seen in the figure, the percent reduction in *C* reduces for each test and can be used as a stopping criterion. Figure 21 shows the posterior cdf after seven updates. Stable results are denoted as 'o' and unstable results as 'x'. Figure 22 and Figure 23 show the progression of μ_C and σ_C as a function of the number of tests. Note that the mean converges to 2.5×10^5 N/m in seven tests.

Table 2. Expected percent reduction at test points.

Test	p(stability)	Expected percent reduction in σ_C
A	0.9	13.8
B	0.51	45.6
C	0.1	14.6
D	0.52	24.9

The experimental selection procedure was repeated for the 19.05 mm diameter, 11 deg relief angle tool. Seven tests were performed at points where the expected percent reduction in σ_C was maximum. Figure 24 shows the posterior cdf. Stable results are denoted as 'o' and unstable results as 'x'. Figures 25 and 26 display the progression of μ_C and σ_C as a function of the number of tests. Note that the mean converges to 3.6×10^5 N/m in seven tests.

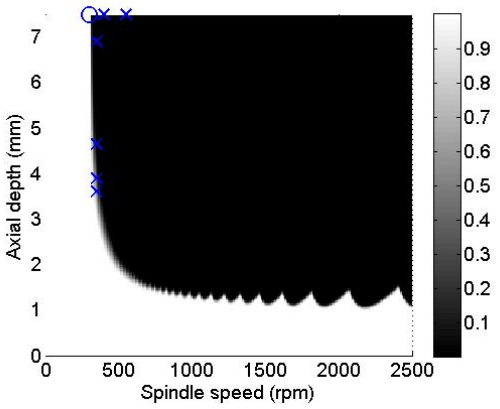

Figure 21. Posterior cdf of stability. Stable results are denoted as 'o' and unstable results as 'x'.

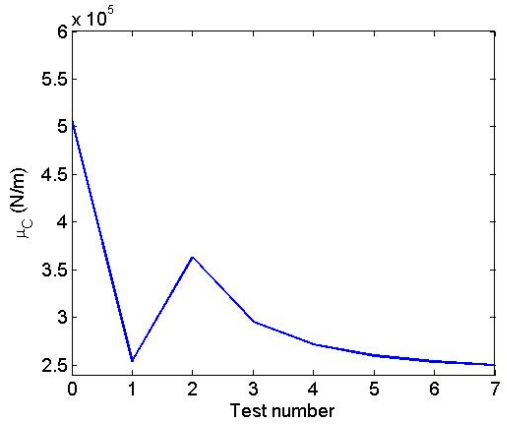

Figure 22. μ_C as a function of the number of tests.

CONCLUSIONS

A random walk method of Bayesian updating was demonstrated for process damping coefficient identification. The prior sample paths were generated using an analytical process damping algorithm. For the prior, each sample stability limit was assumed to be equally likely to be the true stability limit. The probability of the sample stability limit was then updated using experimental results. The updated probabilities of the sample paths were used to determine the posterior process damping coefficient distribution. A value of information was used to select experimental test points which maximized the expected reduction in the process damping coefficient uncertainty.

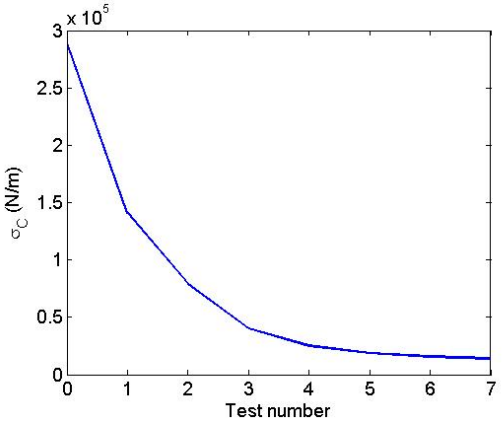

Figure 23. σ_C as a function of the number of tests.

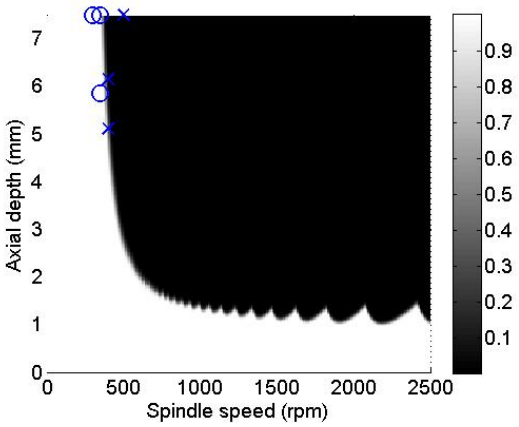

Figure 24. Posterior cdf of stability. Stable results are denoted as ‘o’ and unstable results as ‘x’.

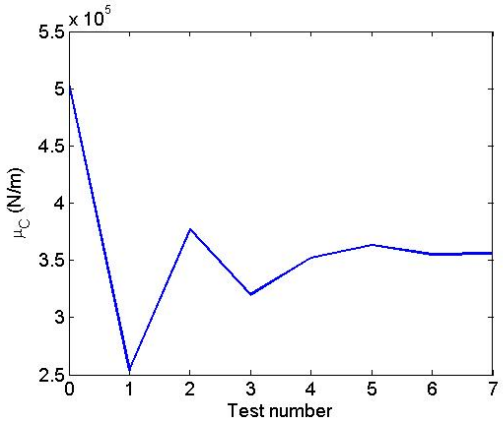

Figure 25. μ_C as a function of the number of tests.

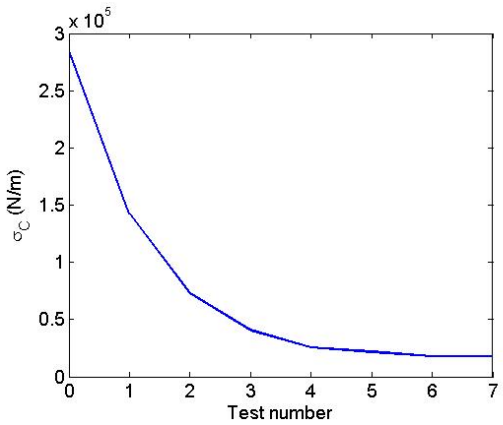

Figure 26. σ_C as a function of the number of tests.

REFERENCES

1. J. Tlusty, M. Polacek, The stability of machine tools against self-excited vibrations in machining, in: Proceedings of the ASME International Research in Production Engineering Conference, Pittsburgh, PA, 1963, pp. 465-474.
2. S.A. Tobias, Machine Tool Vibrations, Blackie and Sons, Ltd., Glasgow, 1965.
3. J. Tlusty, W. Zaton, F. Ismail, Stability lobes in milling, Annals of the CIRP, 32/1 (1983) 309-313.
4. Y. Altintas, E. Budak, Analytical prediction of stability lobes in milling, Annals of the CIRP, 44/1 (1995) 357-362.
5. P.W. Wallace, C. Andrew, Machining forces: Some effects of tool vibration, Journal of Mechanical Engineering Science, 7 (1965) 152-162.
6. T.R. Sisson, R.L. Kegg, An explanation of low-speed chatter effects, Journal of Engineering for Industry, 91 (1969) 951-958.
7. J. Peters, P. Vanherck, H. Van Brussel, The measurement of the dynamic cutting coefficient, Annals of the CIRP, 21/2 (1971) 129-136.
8. J. Tlusty, Analysis of the state of research in cutting dynamics, Annals of the CIRP, 27/2 (1978) 583-589.
9. D.W. Wu, A new approach of formulating the transfer function for dynamic cutting processes, Journal of Engineering for Industry, 111 (1989) 37-47.
10. M.A. Elbestawi, F. Ismail, R. Du, B.C. Ullagaddi, Modelling machining dynamics damping in the tool-workpiece interface, Journal of Engineering for Industry, 116 (1994) 435-439.
11. B.Y. Lee, Y.S. Trang, S.C. Ma, Modeling of the process damping force in chatter vibration, International Journal of Machine Tools and Manufacture, 35 (1995) 951-962.
12. C.Y. Huang, J.J. Wang, Mechanistic modeling of process damping in peripheral milling, Journal of Manufacturing Science and Engineering, 129 (2007) 12-20.
13. K. Ahmadi, F. Ismail, Experimental investigation of process damping nonlinearity in machining chatter, International Journal of Machine Tools and Manufacture, 50 (2010) 1006-1014.
14. E. Budak, L.T. Tunc, A new method for identification and modeling of process damping in machining, Journal of Manufacturing Science and Engineering, 131 (2009) 051019/1-10.
15. Y. Altintas, M. Eynian, H. Onozuka, Identification of dynamic cutting force coefficients and chatter stability with process damping, Annals of the CIRP, 57/1 (2008) 371-374.
16. C. Tyler, T. Schmitz, Process damping analytical stability analysis and validation. Proceedings of NAMRC/SME 40 (2012).
17. J. Tlusty, Manufacturing Processes and Equipment, Prentice Hall, Upper Saddle River, NJ, 2000.
18. T. Schmitz, K.S. Smith, Machining Dynamics: Frequency Response to Improved Productivity, Springer, New York, NY, 2009.